Journal of Building Engineering 98 (2024) 111478

Contents lists available at ScienceDirect

Journal of Building Engineering

journal homepage: www.elsevier.com/locate/jobe

Experimental exploration on impact characteristics of ultra-high performance concrete at low and cryogenic temperature

Kaiyi Chi [a], Jun Li [a], Ruizhe Shao [a], Jian Liu [b,**], Zhongxian Liu [c,***], Chengqing Wu [d,a,*]

[a] School of Civil and Environmental Engineering, University of Technology Sydney, NSW, 2007, Australia
[b] Earthquake Engineering Research and Test Centre, Guangzhou University, Guangzhou, 510405, China
[c] Tianjin Key Laboratory of Civil Structure Protection and Reinforcement, Tianjin Chengjian University, Tianjin, 300384, China
[d] Institute of Rock and Soil Mechanics, Chinese Academy of Sciences, Wuhan, 430071, China

ARTICLE INFO

Keywords:
Low/cryogenic temperature
UHPC
Strain rate effect
Compressive strength
Splitting tensile strength
Dynamic increase factor

ABSTRACT

Concrete structures in polar region and liquefied gas storage system need to be designed against combined low temperature and dynamic loads. Understanding the mechanical behaviour of concrete under these extreme conditions is critical for ensuring the structural integrity and safety. This study presents an experimental investigation on the dynamic compressive and splitting tensile performance of UHPC subjected to low temperatures of −70 °C and −160 °C. The compressive and splitting tensile strengths of UHPC were examined at various strain rates (40–160 s^{-1} for compression, 20–80 s^{-1} for splitting tension) and temperature conditions (at 20, -70 and −160 °C) via Split Hopkinson Pressure Bar (SHPB) device. The dynamic compressive as well as splitting tensile strengths of UHPC increased significantly with rose of the strain rate. The dynamic increase factors in compression (CDIFs) decreased with the decline in temperature. The compressive strength under a strain rate of 120 s^{-1} at ambient temperature were approximately 1.09 and 1.16 times higher than at −70 and −160 °C, respectively. On the other hand, an opposite behaviour was observed for the dynamic increase factors in split tension (TDIFs) of UHPC, i.e., TDIFs rose as the temperature decreased. Based on the experimental data, it showed that the TDIFs at −70 and −160 °C were nearly 1.16 and 1.21 times higher than at 20 °C at the specified strain rate 60 s^{-1}.

1. Introduction

Concrete material is widely used in civil infrastructure under low temperature environments such as All Concrete Liquified Natural Gas (ACLNG) storage tank which exposed to cryogenic temperature around −165 °C [1–3]. These critical structures face threats from dynamic loads, e.g., impact and blast loadings. Consequently, a thorough grasp of the mechanical behaviour and failure mechanisms of concrete across various strain rates is crucial, along with the development of materials and structures capable of enduring dynamic loads and low or cryogenic temperature conditions.

* Corresponding author. School of Civil and Environmental Engineering, University of Technology Sydney, Sydney, NSW, 2007, Australia.
** Corresponding author. Guangzhou University, Guangzhou, 510405, China.
*** Corresponding author. Tianjin Chengjian University, Tianjin, 300384, China.
E-mail addresses: Jian.Liu@gzhu.edu.cn (J. Liu), zhongxian1212@163.com (Z. Liu), cqwu@whrsm.ca.cn (C. Wu).

https://doi.org/10.1016/j.jobe.2024.111478
Received 24 August 2024; Received in revised form 23 November 2024; Accepted 1 December 2024
Available online 5 December 2024

Large number of researches have been devoted to the mechanical properties of normal strength concrete (NSC) at low and cryogenic temperature [4–7]. Rostasy and Wiedemann [8] have conducted a test to investigate the effect of cryogenic temperature to the compressive strength of NSC. The test results indicated that the compressive strength for NSC with Portland cement at −170 °C was approximately three times greater than at 20 °C. Some of the scholars such as Berne [9] and Rostásy and Pusch [10], they analysed the changes of splitting tensile strength of NSC at cryogenic temperature. Their tests results showed that the splitting tensile strength of NSC at −170 °C was roughly two times greater than at 20 °C. A comprehensive literature review been conducted by Van [11], Lin et al. [12] and Huo et al. [13]. The results emphasised an enhancement of NSC performance such as compressive, tensile strength and modulus elasticity etc., which was owing to the phase transition of pore water within the concrete matrix at low/cryogenic temperature. However, concrete under low temperature is more brittle, and prone to cracking [12].

Ultra-high performance concrete (UHPC) emerges as a premium alternative to conventional concrete with its exceptional strength, durability and improved resistance to cracking [14]. Some researchers examined the fundamental mechanical properties of UHPC at low and cryogenic temperature. Kim et al. [15,16] investigated the compressive and tensile behaviour of UHPC at −170 °C. Exposure to extremely low temperatures resulted in a significant enhancement in the mechanical properties of the material. For example, UHPC specimens containing 19.5 mm steel fibres, compressive strength was increased by 46.3 %, tensile strength by 34.4 % and fracture energy by 52.4 % at −170 °C compared to values at ambient temperature. Liu et al. [17] conducted three-point and four-point bending tests to find out the flexural and fracture behaviour of UHPC with temperate ranging from 20 °C to −30, −60, −90, −120 and −160 °C. The flexural peak loads were 1.08, 1.26, 1.28, 1.61, and 1.60 times greater at −30, −60, −90, −120 and −160 °C, respectively, compared to the load at 20 °C with specimen dimension 515 × 100 × 100 (length × height × width in mm). In addition, the fracture energy of UHPC increased by 1.53, 1.61, 1.63, 1.85, and 1.87 times at −30, −60, −90, −120 and −160 °C, respectively, compared to the value at 20 °C. Compared to the experiment results from Xie et al. [18] (who has conducted the three-point bending tests for conventional concrete from 20 °C to −80 °C with the same dimension above), it showed that the fracture energy dramatically increased by 99.38 % and 99.49 % for UHPC specimens at −30 and −60 °C, respectively. The increased fracture resistance of UHPC was attributed to the freezing of pore water into ice, which can enhance the interfacial adhesion between steel fibres and the UHPC matrix. Zhang et al. [19] explored the flexural performance of UHPC under six temperature conditions, ranging from 200 °C to cryogenic temperatures, using acoustic emission (AE) technology to identify cracking characteristics. Results revealed that exposure to in-situ −170 °C signally enhanced flexural strength nearly 2 times greater than the values at room temperature. This improvement was attributed to frozen water acting as a barrier to microcrack propagation, increased frictional resistance from hardened cement grains, and improved bond strength between steel fibres and the cement matrix. However, despite these enhancements, UHPC at −170 °C exhibited reduced ductility, characterised by steeper post-peak load decreased and higher energy release rates. AE results showed stronger signals and a higher proportion of shear cracks in the linear-elastic stage at −170 °C. While at −170 °C condition significantly boosted strength and toughness, it also led to a trade-off in ductility, with the deflection ductility coefficient decreasing by 53.0 % compared to ambient temperature. To address the negative effects of early-age shrinkage, characterised by microcrack formation [20] due to rapid hydration and water loss of UHPC, Jin et al. [21] conducted a study where incorporated 20 % coarse aggregate into traditional UHPC with steel fibre content (0–3%) and tested the mechanical properties, across a wide temperature range from room temperature down to −90 °C. Results indicated a significant improvement in compressive (increased by 46.3 % at −90 °C with 2 % steel fibres compared to 20 °C) and splitting tensile strength (increased by 38.6 % at −90 °C with 2 % steel fibres compared to 20 °C) with decreasing temperature, attributed to improved material properties at lower temperatures and the formation of ice within pores. While steel fibres enhanced compressive and splitting tensile strength, excessive fibre content led to weaken the low-temperature enhancement effect, likely due to fibre agglomeration.

Numerous investigations have examined the dynamic behaviour of UHPC at ambient temperature under both compression [22–25] and tension [26–28]. Su et al. [29] analysed the dynamic behaviour of UHPC. The study stated that the dynamic increase factor (DIF) of UHPC were consistently lower than NSC, and the incorporation of steel fibres evidently impacted the dynamic strength of UHPC. Wu et al. [30] performed Split Hopkinson Pressure Bar (SHPB) test to investigate the impact of hybrid steel fibre reinforcement on the dynamic behaviour of UHPC under compressive strain rate from 100 to 200 s^{-1}. The results showed that fibre with different length exhibited varying crack control capability, and UHPC incorporating a hybrid 1.5 % long fibre and 0.5 % short fibre reinforcements exhibited the optimal mechanical performance. Hou et al. [31] explored the dynamic compressive behaviour of reactive powder concrete (RPC) at strain rates varying from 72 to 317 s^{-1} with different types of fibre reinforcement, the specimens included plain RPC, steel fibre-reinforced RPC (SFRPC) with varying steel fibre content, including PP and steel fibres. The results revealed that plain RPC exhibited greater sensitivity in terms of dynamic compressive strength (f'_c) in contrast to SFRPC. The incorporation of PP fibre slightly decreased the f'_c of SFRPC.

As for the dynamic tensile behaviour of UHPC, Cao et al. [32] conducted a dynamic uniaxial tension test on RPC containing different amounts of steel fibre (plain, 1 % and 2 %) via Split-Hopkinson Tension Bar (SHTB) with high strain rate from 98 to 528 s^{-1}. It indicated that the DIF for tensile strength of RPC rose with higher strain rates and lower steel fibre content. Specifically, DIF in tension varied from 1.0 to 7.5 over the strain rate range of 10^{-6} to 528 s^{-1}. Liu et al. [33] investigated the dynamic splitting tensile strength of UHPC considering the influence for both fibre length (6 and 12 mm) and volume fractions of steel fibres (1.5 %, 2 % as well as 2.5 %) via SHPB tests. It showed that increasing the content and length of steel fibres primarily contributed to an increase in dynamic energy dissipation capacity, with fibre length demonstrating a more significant effect than fibre content.

So far, only a limit study has focused on the dynamic behaviour of concrete material, especially UHPC at low temperature and cryogenic condition, only a few studies have explored in NSC. MacLean and Lloyd [34] performed experiment to investigate the effects of low temperatures (20, 0, −15, −45 and −70 °C) and low strain rates (average strain rate of 1.2 s^{-1}) on the compressive behaviour of concrete by using a drop mass impactor. It showed that the ratio of dynamic to static peak stress decreased linearly with decreasing

temperature, reaching 0.82 at −70 °C. Qiao et al. [35] have conducted dynamic compressive test for NSC at temperatures from 28 °C to −75 °C and strain rates from 34.33 s^{-1} to 63.18 s^{-1} through SHPB tests. They demonstrated that the increase in specific energy absorption (SEA) was more dramatic at lower temperatures, suggesting a stronger temperature enhancement effect, that means, a rise in temperature resulted in an increase in strain rate sensitivity, which may be caused by factors like pore size, saturation level as well as ice crystal formation. The mesoscale numerical model was developed by Jin et al. [36] to capture the complex behaviour of NSC under combined cryogenic temperatures and dynamic loading. It concluded that the strain rate effect in relation to compressive strength was more evident at cryogenic temperatures, and the DIF in compression at −160 °C with a strain rate of 100 s^{-1} was 9.5 % higher in comparison to ambient temperature. Su et al. [37] analysed the dynamic compressive behaviour of concrete via SHPB with strain rate 100 s^{-1} - 300 s^{-1} and built up a mesoscopic model of concrete, including mortar, aggregates, interfacial transition zones (ITZs) as well as ice particles. It emphasised that the improvement of mechanical properties was owing to the effect of ice. The declining temperature led to improved mechanical properties of aggregates and ice, resulting in a gradual decrease in damage rates based on the observation in numerical model. Chi et al. [38] conducted a SHPB test to evaluate the dynamic behaviour regarding normal strength mortar (NSM) at −70 and −160 °C. It was noted that the DIF in compression decreased with reduction in temperature, while the DIFs in tensions rose due to the decline in temperature.

Building upon previous research, this study addresses several gaps in understanding the dynamic behaviour of UHPC, a concrete material with exceptional mechanical properties and durability, in both compression and splitting tension under extreme conditions via SHPB test across the wider range of strain rate. Understanding how UHPC performs under extreme cold temperatures is essential to ensure the structural integrity and safety in low temperature and cryogenic circumstance such as polar areas and energy storage tanks. This research project experimentally examined the dynamic response of UHPC when exposed to low temperatures ranging from −70 to −160 °C. These temperatures were selected to represent the range of extreme cold conditions encountered in various engineering applications.

2. Experimental methodology

The experimental investigation of UHPC dynamic behaviour under low and cryogenic temperatures followed the process in Fig. 1. UHPC specimens were initially produced and subsequently cooled to target temperatures of −70 and −160 °C to simulate low and cryogenic temperature conditions. Two different tests were employed to evaluate the material's mechanical response: static testing and Split Hopkinson Pressure Bar (SHPB) testing, both focusing on compression and splitting tension properties. The static tests provided baseline mechanical properties, while the SHPB tests characterised the dynamic behaviour of UHPC under high strain rates. This dual testing approach enabled a thorough comparison between static and dynamic responses at these extreme temperatures. All experimental data were acquired and analysed to understand the temperature-dependent mechanical properties and strain rate effects on the performance of UHPC under these harsh environmental conditions.

2.1. UHPC specimen preparation and composition

The UHPC specimens were reinforced with 2 % steel fibres. The properties of steel fibre are listed in Table 1. Table 2 provides detailed material proportions. Fig. 2 illustrates the comprehensive particle size distributions of the four solid materials utilised in this UHPC mixture. To ensure optimal dispersion and random orientation of the steel fibres while preventing agglomeration, manual distribution was employed during the fibre incorporation process. Following this step, the concrete mixture was carefully transferred into polyvinyl chloride (PVC) pipe moulds, each with an internal diameter measuring 70 mm. After appropriate curing in the PVC moulds, the samples were cut into cylindrical shapes with a diameter of 70 mm and a height of 35 mm (see Fig. 3). To achieve uniform load distribution during the loading test, the end faces were grinded.

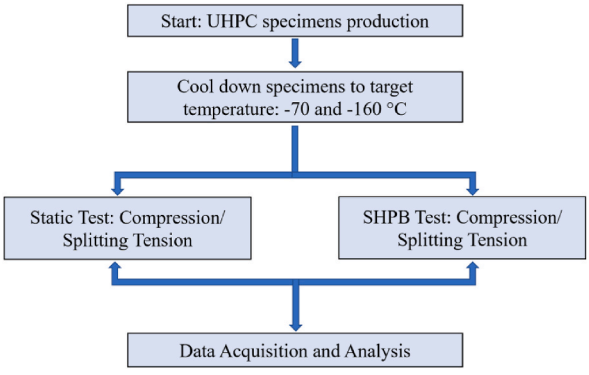

Fig. 1. Experimental methodology for UHPC testing at low and cryogenic temperatures.

Table 1
Material properties of steel fibre.

Diameter (mm)	Length (mm)	Density (kg/m^3)	Modulus elasticity (GPa)	Tensile strength (MPa)
0.12	15	7800	210	>2850

Table 2
UHPC composition ratios (kg/m^3).

42.5 Cement	Water	Fine sand	Steel fibre	Superplasticiser	Fly ash	Silica fume
925	230	963	160	26	340	130

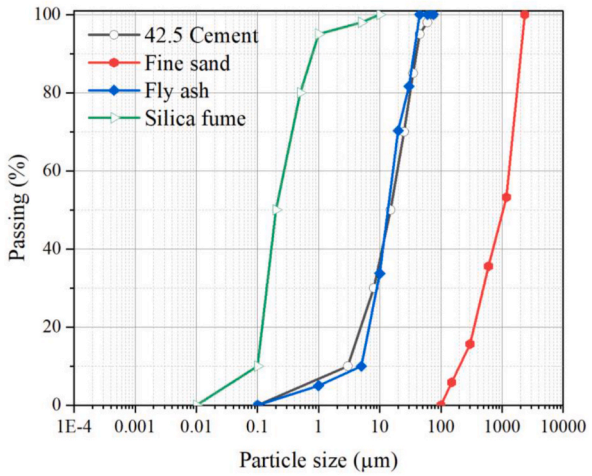

Fig. 2. Particle size distribution of used materials.

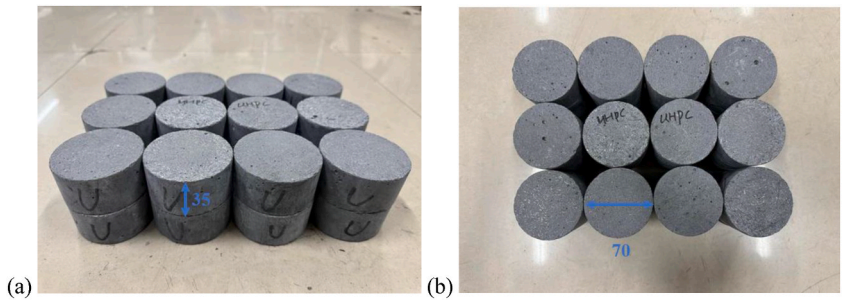

Fig. 3. UHPC specimens for testing (unit: mm).

2.2. Experimental setup under cryogenic temperature

The proposed experiment aims to examine both the static and dynamic compressive and splitting tensile behaviour of UHPC under extreme low temperatures of −70 and −160 °C. To attain the target temperatures, a cooling apparatus as depicted in Fig. 4 was employed. The specimens were put into a low-temperature chamber, which can accommodate 14 specimens simultaneously. The liquid nitrogen was slowly flowed into the low-temperature chamber. During the experiment, the rate of temperature drop was controlled at 1 °C per minute to make sure the uniform temperature distribution within the specimens. The target temperature was maintained for 4 h to guarantee thermal equilibrium. The temperature was accurately recorded and regulated within the low-temperature chamber. Fig. 5 illustrates the cooling curve within the low-temperature chamber.

3. Static test results

The quasi-static experiments were conducted at three distinct temperature conditions, including 20, -70 and −160 °C. A 300-ton

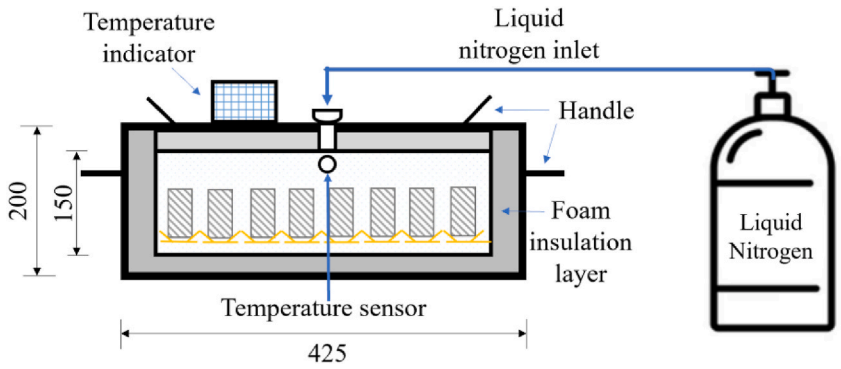

Fig. 4. Test setup of UHPC under cryogenic temperature (unit: mm) [38].

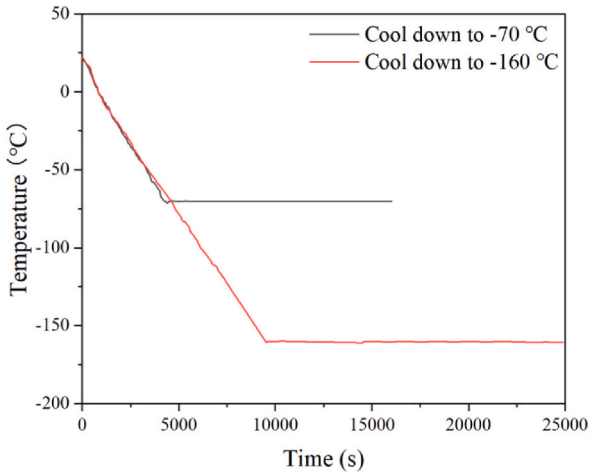

Fig. 5. Cooling curves in the test.

hydraulic testing machine was employed to perform these tests. For the compressive tests, the loading rate was set at 0.5 mm/min. In the case of splitting tensile tests, the cylindrical specimens were placed horizontally between the loading surfaces of the compression testing machine. The compressive load was applied diametrically along the cylinder's length at a slower rate of 0.02 mm/min. This loading continued until failure initiated along the vertical diameter of the specimen.

The static compressive and splitting tensile strengths of UHPC at 20, -70 and −160 °C are shown in Fig. 6. The compressive strength

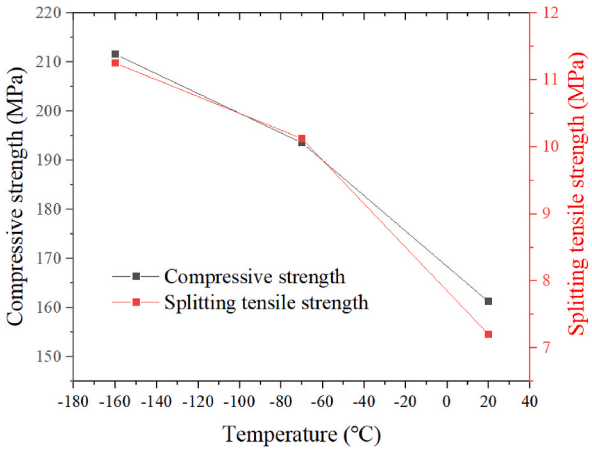

Fig. 6. UHPC Compressive and splitting tensile strength at low temperature.

exhibited an almost linear increase when the temperature decreased from 20 °C to −70 and −160 °C, from 161.20 MPa to 193.56 MPa and 211.58 MPa, respectively, corresponding to an increase of 20.07 % and 31.25 %. Likewise, the splitting tensile strength increased from 7.20 MPa at room temperature to 10.13 MPa and 11.25 MPa at −70 and −160 °C, respectively, representing an increase of 40.69 % and 56.25 %.

4. Split Hopkinson Pressure Bar (SHPB) test setup

The behaviour of UHPC under dynamic compression and splitting tensile loading at various strain rates and low/cryogenic temperatures was explored experimentally. Dynamic compressive tests were conducted at strain rates of 40, 80, 120 and 160 s^{-1}, while splitting tensile tests were performed at strain rates of 20, 40, 60 and 80 s^{-1}. Notably, these tests were carried out at three distinct temperature conditions, including 20, -70 as well as −160 °C. The specimens employed for the experiment were cylindrical, having dimensions of 35 mm in height and 70 mm in diameter.

The SHPB configuration for conducting dynamic compressive as well as splitting tensile tests is depicted in Fig. 7. This apparatus consisted of two long, slender bars (termed the incident and transmission bars) with the test specimen sandwiched between their ends. Proper alignment of all components, including the striker bar, incident bar, transmission bar as well as buffer bar, was crucial before commencing the experiment to ensure coaxial loading conditions.

Strain gauges strategically positioned on both incident and transmission bars enabled the measurement of the elastic strain pulses induced by the incident, reflected as well as transmitted waves, respectively. The acquired data can be used in conjunction with one-dimensional elastic wave theory [39–41], to derive the stress-strain relationship in SHPB compressive test through the following equations.

$$\sigma = \frac{EA_e}{2A_s}(\varepsilon_i + \varepsilon_r + \varepsilon_t) \tag{1}$$

$$\varepsilon(t) = -\frac{2C_0}{L}\int_0^t \varepsilon_r(t)dt \tag{2}$$

$$\dot{\varepsilon}(t) = -\frac{2C_0}{L}\varepsilon_r(t) \tag{3}$$

where σ represents the stress at the interface where the specimen and loading bar meet; E denotes the modulus elasticity of the incident and transmission bars; A_e and A_s symbolise the cross-section area of the pressure bar and sample, respectively. $\varepsilon_i, \varepsilon_r$ and ε_t correspond to the incident, reflected, and transmitted wave pulses, respectively. C_0, L and t signify the longitude wave velocity of incident/transmission bars, the initial length of the specimen and time, respectively.

During dynamic splitting tests, the specimen was positioned along the radial direction, with the incident and transmission bars gripping the two opposing side surfaces of the specimen. Utilising the principles of one-dimensional stress wave theory, the stress, strain, as well as strain rate for the SHPB splitting tensile test could be mathematically derived in the following equations.

$$\sigma = \frac{2P(t)}{\pi DL} = \frac{2EA_e\varepsilon_t(t)}{\pi DL} \tag{4}$$

$$\varepsilon(t) = -\frac{2C_0}{D}\int_0^t \varepsilon_r(t)dt \tag{5}$$

$$\dot{\varepsilon}(t) = -\frac{2C_0}{D}\varepsilon_r(t) \tag{6}$$

where D denotes the original diameter of the specimen prior to testing, while the other variables have been previously defined.

During the splitting tensile tests, the contact interface between the specimen and the bars was effectively a line, resulting in a relatively weaker transmitted wave signal as compared to the compressive tests.

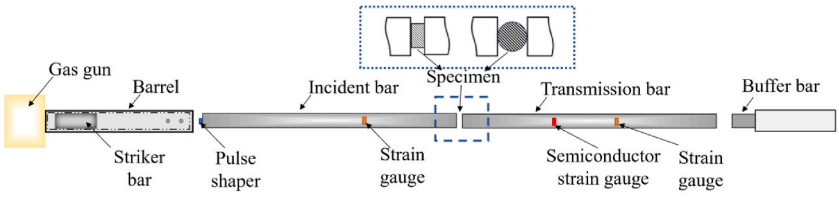

Fig. 7. SHPB test setup [38].

5. Results and discussions of experiments

5.1. Dynamic compressive test

5.1.1. Damage appearances of specimens subjected to coupled loading

Fig. 8 presents the dynamic compressive failure modes of UHPC specimens at different temperatures and strain rates. At 20 °C (see Fig. 8(a)), the specimens exhibited a progressive increase in damage severity as the strain rate rose. At the lowest strain rate of 40.7 s^{-1}, the specimen showed moderate damage with some cracking and chipping. When the strain rate rose to 81.4 s^{-1}, the sample exhibited pronounced cracking and fragmentation. At 120.1 s^{-1}, the specimen appeared severely damaged, with substantial fragmentation and the formation of smaller debris, the UHPC demonstrated superior damage resistance compared to Normal Strength Mortar (NSM) [38], as evidenced by its central core remaining relatively intact, which was caused by the effect of steel fibres. Finally, at the highest strain rate of 158.2 s^{-1}, the specimen disintegrated into powdery fragments, indicating complete failure. At −70 °C (see Fig. 8(b)), a similar trend was observed, but the overall damage appeared less severe with respect to the state of ambient temperature. The specimens at lower strain rates (39.1 s^{-1} and 81.6 s^{-1}) showed moderate cracking and edge chipping, while the core retained relatively intact. At 121.3 s^{-1}, the specimen exhibited more significant fragmentation, with the formation of granular debris. At the highest strain rate of 162.6 s^{-1}, the specimen disintegrated into smaller fragments, but less severe damage occurred in contrast with the corresponding specimen at 20 °C. While at −160 °C (see Fig. 8(c)), the specimens demonstrated even higher resistance to dynamic compressive failure. The specimens at lower strain rates (45.2 s^{-1} and 82.3 s^{-1}) exhibited minimal damage, with only minor cracking visible. At 119.2 s^{-1}, the specimen showed moderate fragmentation, but the core remained largely intact owing to simultaneous action of steel fibres, albeit with signal cracking and fragmentation. However, at the highest strain rate of 161.5 s^{-1}, the specimen exhibited more severe damage and disintegration in comparison with the corresponding specimens at 20 °C and −70 °C. This may show the increased brittleness of UHPC at lower temperature at higher strain rate.

Overall, it highlighted the significant impact of both thermal conditions and strain rate on the dynamic compressive failure mechanisms of UHPC. Lower temperatures especially at −160 °C resulted in improved resistance to damage and fragmentation at the lower strain rates (40 and 80 s^{-1}), but more brittle at higher strain rate.

The dynamic failure process of UHPC specimens under compressive loading at different temperatures (20, −70 and −160 °C) was captured via ultra-high-speed video camera (see Fig. 9). It can be observed that at 57 μs, more obvious cracks appeared in the −160 °C sample, as compared to room temperature and −70 °C. Over time, the damage to the sample at −160 °C became more severe, accompanied by a large amount of powder and small fragments. This observation highlighted the impact of temperature on the mechanical properties and failure behaviour of UHPC, with lower temperatures resulting in a more brittle and catastrophic failure

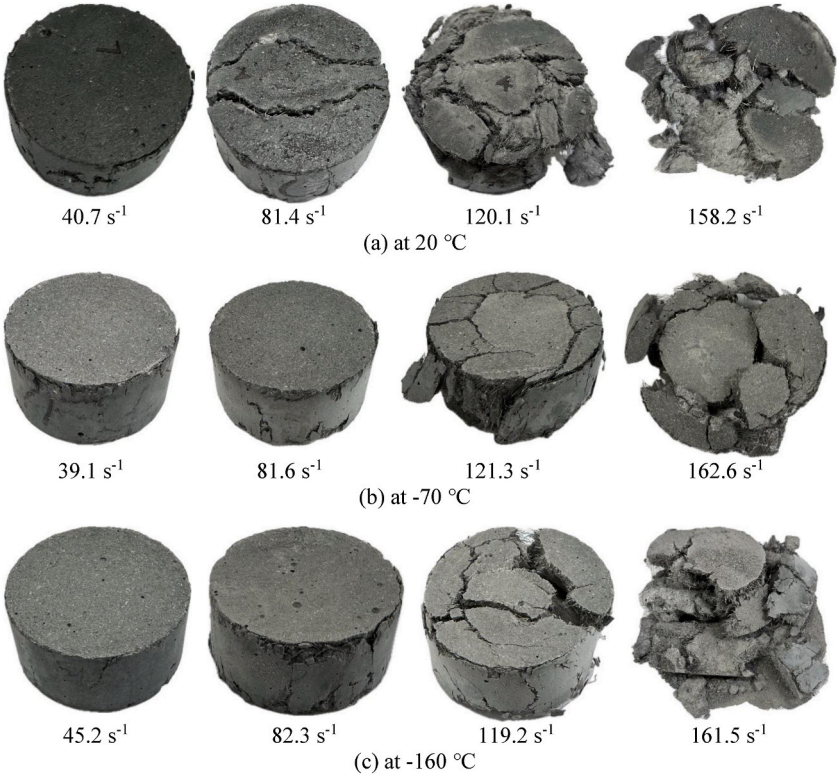

Fig. 8. Dynamic compressive failure patterns of UHPC across various temperatures.

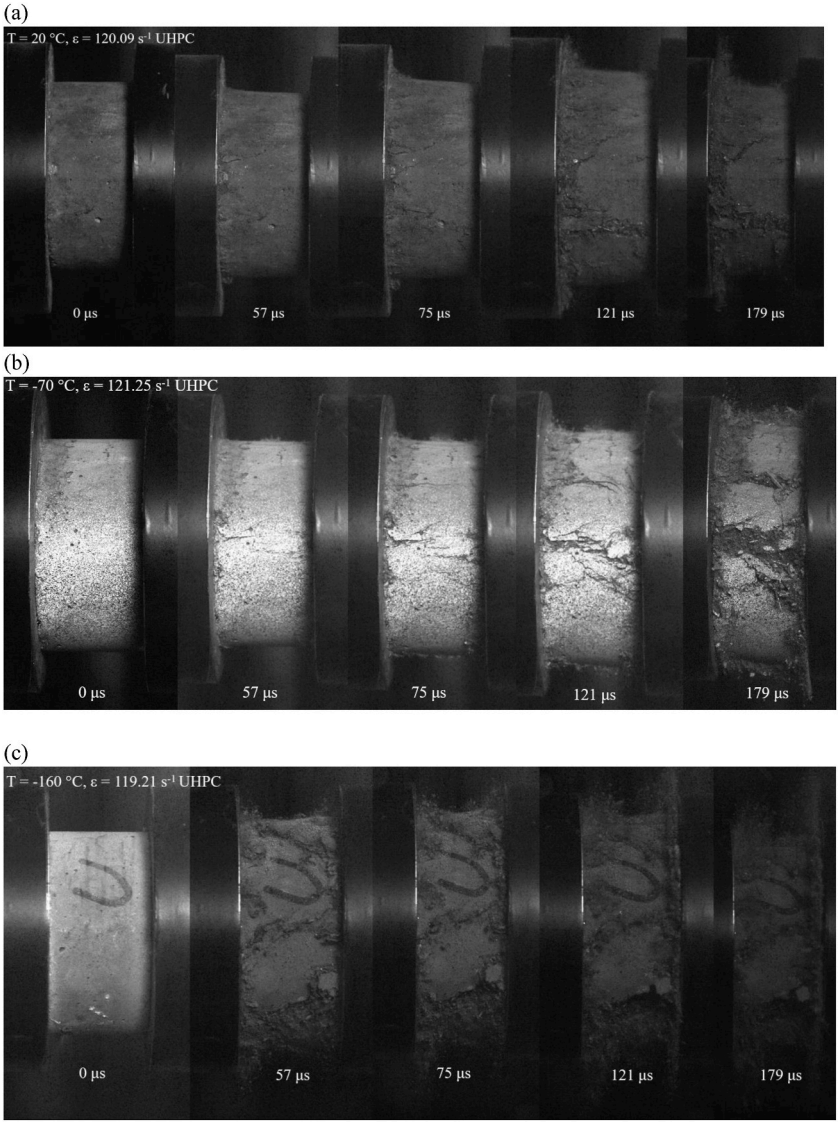

Fig. 9. Failure process of UHPC at various temperature. (a) at 20 °C (b) at −70 °C (c) at −160 °C.

mode at higher strain rate.

UHPC was a dense, homogeneous material [42] with a tightly packed microstructure and a high degree of hydration, which contributed to its superior mechanical performances and resistance to cracking and fragmentation under impact loading. Wu et al. [43] examined the microstructure of the matrix by Mercury intrusion porosimetry (MIP) and showed that after adding fly ash and other substances, the total porosity of the UHPC matrix decreased by about 5 %. The filling effect of supplementary cementitious materials (SCMs) densified the UHPC matrix, resulting in improved mechanical properties. At lower temperatures, the stiffness of UHPC increased due to the phase change in the free water, resulting in the enhancement of compressive strength. However, it should emphasise that as concrete's strength increased, it typically became more prone to brittle failure [44]. Even when steel fibres were incorporated into mixtures, UHPC still exhibited brittle failure modes when subjected to extremely low temperatures [16,45]. Therefore, it showed noticeably more brittle failure characteristics at −160 °C compared to room temperature and −70 °C.

The frozen-pore water effect at cryogenic temperatures enhanced the bond between steel fibres and the cement matrix, thereby restricting crack propagation. Kim and Yoo [46] examined how cryogenic temperatures affected the pull-out characteristics of individual steel fibres embedded in UHPC matrix. They pointed out that exposure to extremely low temperatures considerably improved both the average bond strength and slip capacity, contributing to the strength enhancement. Overall, it exhibited the superior performance of UHPC in terms of damage resistance and controlled failure modes.

5.1.2. Effect of low temperature on compressive strength and modulus of elasticity

Fig. 10 demonstrates the relationship between dynamic compressive stress and strain for UHPC specimens tested at various temperatures (20, −70 and −160 °C) and strain rates (ranging from 40 s^{-1} to 160 s^{-1}). At the ambient temperature, the dynamic peak stress of UHPC increased signally with rising strain rate. Specifically, the f'_c increased by 16.4 %, 32.0 %, 47.3 % and 52.1 % at strain rates of 40.7 s^{-1}, 81.4 s^{-1}, 120.1 s^{-1} and 158.2 s^{-1}, respectively, in comparison with the static strength (see Fig. 10(a)). At −70 °C, the stress-strain curves exhibited a similar trend as those at room temperature, with the peak stresses kept increasing at higher strain rates. By comparing the static strength at −70 °C, the dynamic compressive strength escalated by 5.2 %, 22.9 %, 34.7 % and 35.3 % at strain rates of 39.1 s^{-1}, 81.6 s^{-1}, 121.3 s^{-1}, and 162.6 s^{-1}, respectively (see Fig. 10(b)).

At −160 °C, the stress-strain curves exhibited a more brittle behaviour with a steeper post-peak softening branch as compared to 20 and -70 °C. The f'_c continued to increase with strain rate. At the strain rate of 45.2 s^{-1}, 82.3 s^{-1}, 119.2 s^{-1} and 161.5 s^{-1}, the dynamic compressive strength at −160 °C experienced an increase of 1.66 %, 13.1 %, 26.7 % and 29.8 % in contrast to the uniaxial compressive strength at −160 °C. These findings demonstrated that the f'_c of UHPC specimens increased with strain rate across all temperature conditions. This trend was particularly pronounced at room temperature, where the strength enhancement was more substantial as compared to −70 °C and −160 °C. As the temperature reduced from −15 °C to −125 °C and below, Wu and Prakash [47] observed an increase peak stress of ice, resulting in an enhancement of compressive strength for UHPC with declined temperature.

Regarding the dynamic compressive modulus elasticity of UHPC, a phenomenon similar to that observed in NSM [38] was noted, i.e., the dynamic modulus elasticity at −70 °C was higher than that at room temperature and −160 °C. According to Zhang et al. [48], this is probably caused by the binding and filling actions of ice in the pores of the concrete in this temperature range. The formation of ice in the pores helped fill the voids and bind the cement paste and aggregates together, causing an increase in the overall stiffness and modulus elasticity of the UHPC. Additionally, the thermal contraction of the UHPC components at −70 °C further contributed to this stiffening effect, as it reduced the volume of the pores and raised the density of the material. However, as the temperature was dropped further down to −160 °C, the dynamic elastic modulus started to decrease. This can be explained by the increased thermal expansion mismatch between the different UHPC constituents (cement paste, aggregates, and ice) at cryogenic temperatures. The inconsistent thermal deformations resulted in the development of microcracks and damage within the UHPC microstructure, which in turn reduced the overall stiffness and dynamic elastic modulus of the material. At the strain rate of about 120 s^{-1}, the dynamic elastic modulus of UHPC at −70 °C was approximately 7.16 times and 3.64 times higher than at 20 °C and −160 °C, respectively. This highlighted the markedly influence of the ice filling and binding effects as well as the thermal expansion mismatch on the dynamic mechanical performances of UHPC at different low and extremely low temperature conditions.

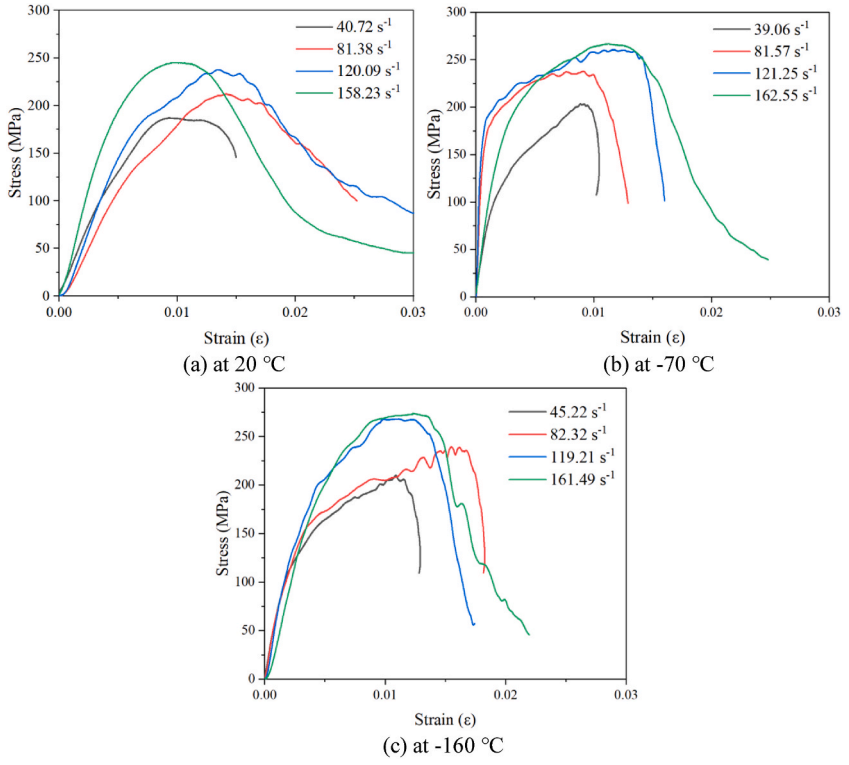

Fig. 10. Dynamic compressive stress-strain curve at various temperatures.

5.2. Dynamic splitting tensile results

5.2.1. Failure modes of specimens under combined loading

Fig. 11 illustrates the dynamic splitting tensile failure modes of UHPC specimens at various temperatures and strain rates. The relationship among temperature, strain rate, and the resulting damage patterns in the concrete specimens were examined. At various strain rates (20, 40, 60 and 80 s^{-1}) and temperatures (20, −70 and −160 °C), different failure modes appeared in the specimens. Three primary categories may be used to classify the failure scenarios [49]: Failure Mode I (lower strain rates): The specimen maintains stress equilibrium before cracking, then splits from the centre along the loading axis into two halves that can be reassembled to closely resemble the original shape. Failure Mode II (above 20 s^{-1}): The specimen experiences a fracture along its central axis, resulting in two distinct halves. A minor wedge-shaped zone of crushing is evident at the point of load application. Failure Mode III: The specimen exhibits a more complex failure pattern. Shear damage manifests at both extremities of the specimen. Concurrently, a wedge-shaped crushing zone develops at the loading end. The central region of the specimen displays a substantial zone of tensile damage, often presenting as a band of crushed material. At lower strain rates (around 20 s^{-1}), the specimens exhibit a central crack damage pattern, where they fracture into two halves along the loading direction. At higher strain rates (above 20 s^{-1}), the specimens display a triangular crack damage pattern, characterised by triangular damage zones, especially at the contact ends (particularly the loading end). The damage level escalated with strain rate, with the triangular fracture area expanding and the overall deformation increasing. Generally speaking, the transition in failure modes observed in the UHPC specimens, shifting from shear failure to tensile failure, can be primarily attributed to the redistribution of maximum tensile strain within the material [50]. A comparative assessment revealed that, under identical strain rates, the extent of damage was more severe at −70 °C than at ambient temperature. Furthermore, the damage severity at −160 °C was even worse than at −70 °C.

Fig. 12 shows the failure process of UHPC under dynamic splitting tensile tests conducted at approximately 40 s^{-1} strain rate together with temperatures of 20, -70 and −160 °C. As time progressed, the cracks in the UHPC specimens propagated along the centre of the samples, gradually widening and extending. At −70 °C, an undamaged sample displayed at 33 μs, while a more rapid and irregular crack propagation pattern demonstrated at the following time step 82 μs, 112 μs and 180 μs in contrast to the state of room temperature. At the temperature of −160 °C, the failure of UHPC became more sudden and catastrophic, exhibiting a more brittle behaviour. The crack formation was visible as early as 8 μs, with subsequent widening and extension of the crack at 33 μs, 112 μs and 180 μs In summary, as the temperature decreased, the crack initiation and propagation become more rapid, irregular, and

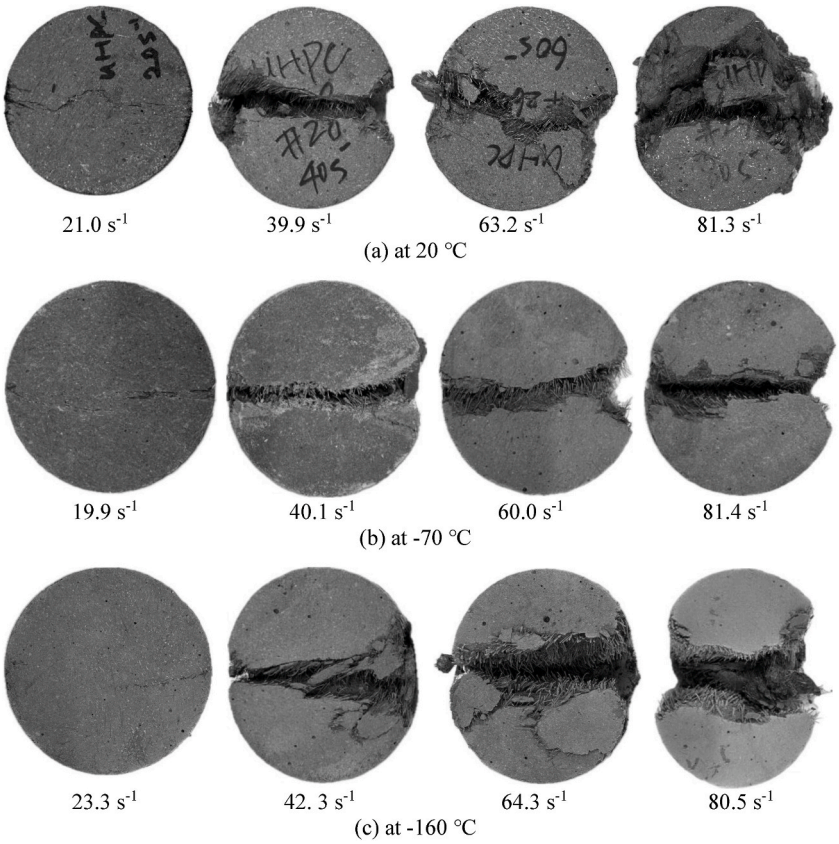

Fig. 11. Dynamic splitting tensile failure mechanisms of UHPC at various temperatures.

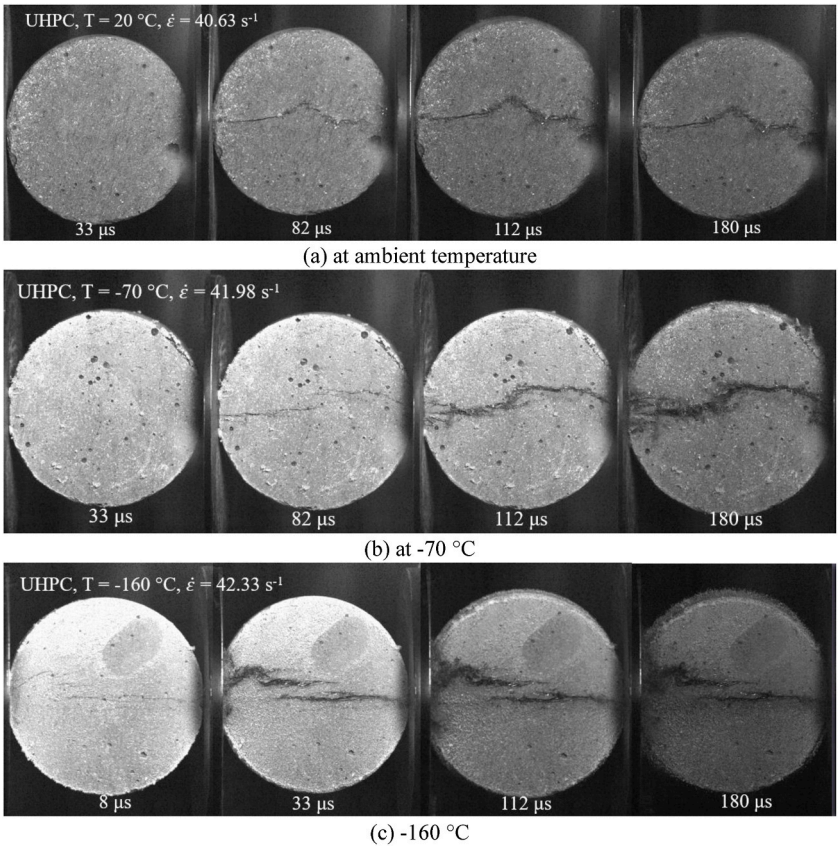

Fig. 12. Failure process of UHPC under dynamic splitting tensile test.

catastrophic, indicating a transition from a more ductile failure mode at ambient temperature to a more brittle failure mode at lower temperatures.

5.2.2. Effect of low temperature on splitting tensile strength

The dynamic splitting tensile behaviour of UHPC was investigated at temperature conditions of 20, -70 and −160 °C, with strain rates ranging from approximately 20 to 80 s^{-1}, and the peak splitting tensile strength of different scenarios is presented in Fig. 13. At room temperature, as the strain rate increased from 21.0 s^{-1} to 39.9 s^{-1}, 63.2 s^{-1}, and 81.3 s^{-1}, the splitting tensile strength of the

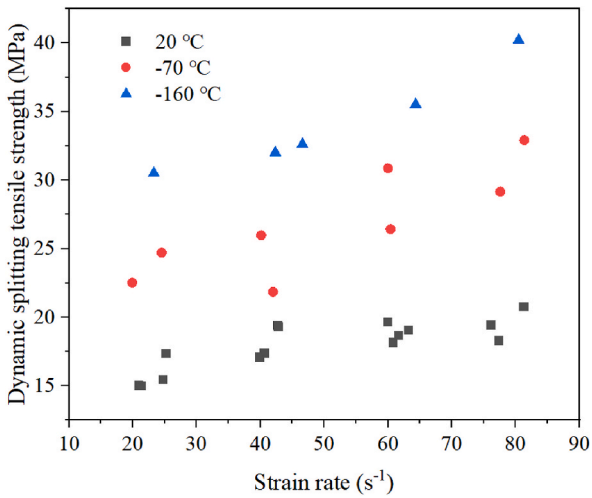

Fig. 13. Dynamic splitting tensile strength of UHPC at various temperatures.

UHPC specimens rose by approximately 108.6 %, 141.1 %, 172.6 % and 188.1 %, respectively, in contrast to the static splitting tensile strength at 20 °C. At −70 °C, with increasing strain rates from 19.9 s^{-1} to 40 s^{-1}, 60.0 s^{-1} and 81.4 s^{-1}, the splitting tensile strength showed respective increases of about 122.3 %, 156.5 %, 204.6 % and 224.9 % in compared to the static splitting tensile strength at −70 °C. Similarly, at −160 °C, with strain rates rising from 23.3 s^{-1} to 42.3, 63.3 and 80.5 s^{-1}, the splitting tensile strength exhibited increase of around 171.20 %, 184.6 %, 215.7 % and 257.5 %, respectively, in contrast with the static splitting tensile strength at −160 °C. It was noted that as the strain rate ascended, the splitting tensile strength of the specimen increased at the same temperature condition. Furthermore, it was evident that under the same strain rate the dynamic splitting tensile strength rose as the temperature decreased. For example, at a strain rate of 40 s^{-1}, the dynamic splitting strength at −70 and −160 °C rose by 52.3 % as well as 87.7 %, respectively. Likewise, at strain rates of 80 s^{-1}, the dynamic splitting tensile strength at −70 and −160 °C grew to 58.7 % as well as 93.9 %, respectively, as compared to room temperature.

5.3. Relationship between dynamic compressive and splitting tensile strength

The relationship between dynamic compressive strength and splitting tensile strength at various temperatures and strain rates can be expressed using Equation (7). This equation incorporates the effects of strain rate and temperature at 20, -70 and −160 °C on the material's mechanical properties. These relationships were established through regression analysis, having high correlation coefficient of determination (R^2), which was 0.87, 0.91 and 0.92 at 20, -70 and −160 °C, respectively. This indicates a strong fit between the predicted and experimental values. These findings highlight the significant influence of strain rate and temperature on the dynamic compressive and tensile properties of UHPC, showing their interdependence under varying conditions.

$$f'_{c,d}=\begin{cases} 25.92\ln\dot{\varepsilon}+5\times10^{-4}f'_{t,d}+100 & T=20\,^{\circ}C \\ 33.97\ln\dot{\varepsilon}+1\times10^{-4}f'_{t,d}+100 & T=-70\,^{\circ}C \\ 38.27\ln\dot{\varepsilon}+1.34f'_{t,d} & T=-160\,^{\circ}C \end{cases} \tag{7}$$

where $f'_{c,d}$ is the dynamic compressive strength in MPa, $\dot{\varepsilon}$ is the strain rate in s^{-1} and $f'_{t,d}$ represents the dynamic splitting tensile strength in MPa.

6. Strain rate sensitivity

The dynamic increase factor (DIF) is a widely utilised metric that quantifies the enhancement in concrete's strength at high strain rates. The definition of DIF is the proportion of dynamic strength to static strength. Understanding DIF of concrete is crucial for accurately predicting the structural response, designing structural elements to withstand high-strain-rate events, and developing appropriate constitutive models. In accordance with the foregoing experiment results, the relationship between strain rate in compression of UHPC and dynamic increase factor in compression (CDIF) is plotted in Fig. 14. It is worth noting that with the decline in temperature, CDIFs decreased gradually, which indicated the concrete material was more sensitive at ambient temperature rather than at low or cryogenic temperature in compression.

In fact, a large number of empirical formulas for NSC under different strain rate ranges have been derived and widely used. The predictive curve suggested by CEB-FIP model code [51] for DIF in compression at room temperature is given in Equation (8), which also plots in Fig. 14. However, as mentioned above, this formula can only describe the critical strain rate for NSC at ambient

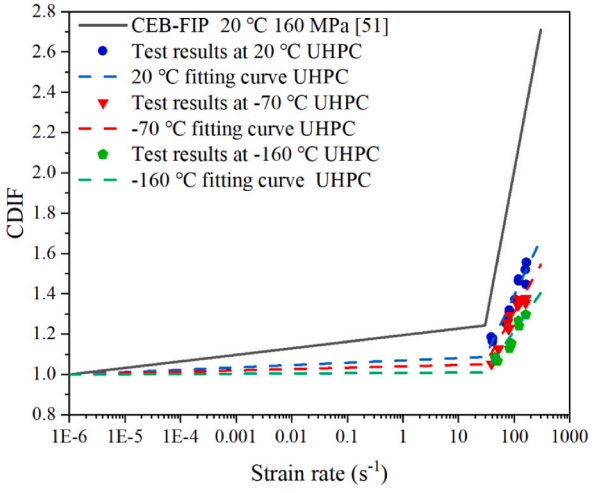

Fig. 14. CDIFs for UHPC at low temperature.

temperature, in other words, it was not suitable for UHPC at other temperature conditions. Therefore, new empirical formulas were derived for UHPC at room temperature, −70 and −160 °C using experimental data, as shown in Equations (9)–(11). The derived empirical formulae fit well with the experimental data. In the current study, the inflection points in relation to CDIF were determined to be 30 s^{-1} at 20, -70 and −160 °C, which was the same as CEB-FIP model code [51].

$$DIF = \frac{f_c}{f_c'} = \begin{cases} \left(\frac{\dot{\varepsilon}}{\varepsilon_s}\right)^{1.026\alpha} & \text{for } \dot{\varepsilon} \le 30\ s^{-1} \\ \gamma\left(\frac{\dot{\varepsilon}}{\varepsilon_s}\right)^{1/3} & \text{for } \dot{\varepsilon} > 30\ s^{-1} \end{cases} \tag{8}$$

where $\varepsilon_s = 3 \times 10^{-6}\ s^{-1}$, $\alpha = \frac{1}{10+6f_c'/10}$ and f_c' is uniaxial compressive strength, $\gamma = 10^{(7.11\alpha - 2.33)}$.

The fitting curves of CDIFs for UHPC at 20, -70 and −160 °C are also displayed in Fig. 14. It was highlighted that with the decrease in the temperature, the CDIFs of UHPC diminished. In fact, the material with a higher uniaxial compressive strength shows lower rate sensitivity [52,53], this align with the observation of UHPC's CDIF at low temperature. The occurrence of a phase transition within the pore network, wherein the pore water crystallised into an ice matrix upon exposure to cryogenic conditions [54]. It is noteworthy that at a temperature of −70 °C, the ice has not yet assumed complete control over its impact on the compressive strength, as the freezing process has merely initiated within the pores [55]. Upon further cooling to −160 °C, the ice within the pores becomes remarkably more rigid, freezing water further expands, leading to microcracking and weakening of the concrete matrix. As temperature decreases, different components of UHPC contract at different rates, forming the microcrack in the ITZ [2]. Meanwhile, the freezing of water within the concrete's pore structure leads to a volumetric expansion of about 9 % [56]. This expansion contradicts the overall shrinkage of the surrounding matrix, exacerbating the development of microcracks. These microcracks serves as initial defects. When subjected to impact loads, these initial defects rapidly coalesce into larger macrocracks, accelerating the path to ultimate failure, hence the CDIF under low temperatures is reduced.

$$\text{CDIF at } 20\ ^\circ C = \begin{cases} 0.012\log\dot{\varepsilon} + 1.070 & \dot{\varepsilon} \le 30\ s^{-1} \\ 0.580\log\dot{\varepsilon} + 0.230 & \dot{\varepsilon} > 30\ s^{-1} \end{cases} \tag{9}$$

$$\text{CDIF at } -70\ ^\circ C = \begin{cases} 0.007\log\dot{\varepsilon} + 1.041 & \dot{\varepsilon} \le 30\ s^{-1} \\ 0.527\log\dot{\varepsilon} + 0.238 & \dot{\varepsilon} > 30\ s^{-1} \end{cases} \tag{10}$$

$$\text{CDIF at } -160\ ^\circ C = \begin{cases} 0.001\log\dot{\varepsilon} + 1.008 & \dot{\varepsilon} \le 30\ s^{-1} \\ 0.427\log\dot{\varepsilon} + 0.349 & \dot{\varepsilon} > 30\ s^{-1} \end{cases} \tag{11}$$

A unified model was utilised to gain a single equation to understand how DIF changed not only with strain rate but also with temperature in a continuous manner. It also enabled to predict DIF values for temperatures and strain rates that were not directly tested. The following Equation (12) was obtained based on the experimental results in Appendix A. Fig. 15 compares the outcomes of Equation (11) with the experimental results presented in Appendix A. The coefficient of determination (R^2) values was 0.96, which indicated a strong correlation between the forecasted and observed CDIFs, supporting a reliability and accuracy of the prediction formula.

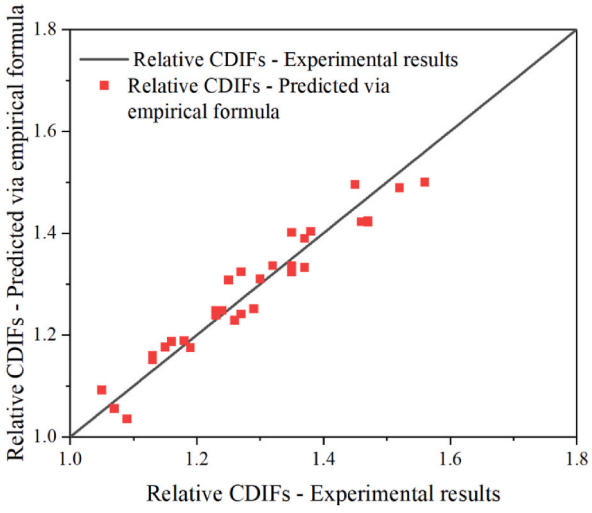

Fig. 15. Comparison of predicted CDIFs to experimental results.

$$\mathrm{CDIF} = 0.557 + 0.001 \times T + 0.284 \times \log\dot{\varepsilon} + 0.059 \times (\log\dot{\varepsilon})^2 + 0.0001 \times T \times \log\dot{\varepsilon} \tag{12}$$

where T symbolises temperature in °C, $-160\ ^\circ\mathrm{C} \le T \le 20\ ^\circ\mathrm{C}$; $\dot{\varepsilon}$ represents as the strain rate, $38.5\ \mathrm{s}^{-1} \le \dot{\varepsilon} \le 165.81\ \mathrm{s}^{-1}$.

Fig. 16 depicts the aggregated data and estimates for the TDIFs of UHPC. The figure also compared the experimental data with the models proposed by CEB-FIP model code [51] as Equation (13) and Malvar and Crawford [57] as Equation (14), both of which used uniaxial compressive strength of 160 MPa at room temperature. It revealed that neither the CEB-FIP model code [51] nor Malvar and Crawford [57] adequately described the TDIFs of UHPC at high strain rates. The inflection points, which represented the transition from the static to the dynamic regime, also did not align well with the observed data. The CEB-FIP model predicted an inflection point at 30 s^{-1}, while the Malvar and Crawford model suggested an inflection point at 1 s^{-1}, both of which did not match the experimental findings. In contrast, Park et al. [58] proposed a different relationship for the TDIFs of UHPC, with a reported transition strain rate of 25 s^{-1}. Furthermore, Yang et al. [59] have pointed out that the inflection point in the DIF-strain rate relationship can be influenced by various factors, like the fibre shape (straight, twisted, or hooked), matrix strength and fibre volume fraction. In the current study, the inflection points were determined to be 1 s^{-1} at 20, -70 and −160 °C, the same as Malvar and Crawford [57].

$$DIF = \frac{f_T}{f_{Ts}} = \begin{cases} \left(\dfrac{\dot{\varepsilon}}{\dot{\varepsilon}_s}\right)^{1.016\alpha} & \text{for } \dot{\varepsilon} \le 30\ \mathrm{s}^{-1} \\ \gamma\left(\dfrac{\dot{\varepsilon}}{\dot{\varepsilon}_s}\right)^{1/3} & \text{for } \dot{\varepsilon} > 30\ \mathrm{s}^{-1} \end{cases} \tag{13}$$

where ε_s is equal to $3 \times 10^{-6}\ \mathrm{s}^{-1}$, $\alpha = \frac{1}{10+6f_c'/10}$ and f_c' is uniaxial compressive strength, $\gamma = 10^{(7.11\alpha - 2.33)}$.

$$DIF = \frac{f_T}{f_{Ts}} = \begin{cases} \left(\dfrac{\dot{\varepsilon}}{\dot{\varepsilon}_s}\right)^{\delta} & \text{for } \dot{\varepsilon} \le 1\ \mathrm{s}^{-1} \\ \beta\left(\dfrac{\dot{\varepsilon}}{\dot{\varepsilon}_s}\right)^{1/3} & \text{for } \dot{\varepsilon} > 1\ \mathrm{s}^{-1} \end{cases} \tag{14}$$

where f_T and f_{Ts} represent the dynamic as well as static tensile strength, respectively. $10^{-6} \le \dot{\varepsilon} \le 160\ \mathrm{s}^{-1}$, $\dot{\varepsilon}_s = 1 \times 10^{-6}\ \mathrm{s}^{-1}$, $\delta = \frac{1}{1+8f_c'/10}$, f_c' is uniaxial compressive strength and $\log\beta = 6\delta - 2$.

The empirical formulae of TDIFs for UHPC at 20, -70 and −160 °C were derived and showed in Equations (15)–(17). The fitting curve for each temperature presents in Fig. 16. It demonstrated that the empirical formula derived in the study could accurately match the experimental data for the TDIFs of UHPC, indicating a high degree of precision and reliable predictive capabilities for model. It can be observed that with decrease in temperature, the TDIFs increased dramatically for UHPC, showing the highest rate sensitivity at −160 °C. At a strain rate of approximately 20 s^{-1}, the TDIFs of UHPC at ambient temperature were 11.00 % and 35.50 % lower than at −70 and −160 °C, respectively. In addition, the TDIFs of UHPC at −70 and −160 °C exceeded those at ambient temperature by 11.26 % and 23.38 % at a strain rate nearly 40 s^{-1}. Similarly, at a strain rate of around 60 s^{-1}, the TDIFs of UHPC were 7.19 % lower at ambient temperature than at −70 °C, and 28.01 % lower than at −160 °C. The TDIFs of UHPC in specific strain rate 80 s^{-1} at −70 and −160 °C had a spectacular rise of nearly 17.33 % and 29.24 % compared with those at the room temperature, respectively. The TDIFs of UHPC showed an increasing tendency as the temperature decreased, indicating a high sensitivity to strain rate under lower temperature conditions.

The hypothesis for this phenomenon is as follows. As temperatures drop, ice crystals progressively form within the micro-cracks and pores of the concrete. These ice formations act as natural bridges across the micro-cracks and strengthen the bond between aggregate particles and the surrounding cement paste [54]. As water in the pores freezes, it forms an ice skeleton within the concrete microstructure. This ice network can effectively enhance the internal structure of the concrete at low temperatures. The pre-stressed state induced by the formation of the ice veins can retard or inhibit the initiation and growth of internal cracks within the material. On the other hand, the bond between steel fibres and the concrete matrix improves at lower temperatures [16,46]. This enhancement is primarily attributed to the increased frictional resistance that develops under cryogenic conditions. A comparison between NSM [38] and UHPC at cryogenic conditions (−160 °C) and a high strain rate (80 s^{-1}) revealed a significant difference in the TDIF. It found that the TDIF of NSM which data based on the results from Chi et al. [38] was 1.61 times greater than that of UHPC under −160 °C at the strain rate of 80 s^{-1}. It was important to note that the primary distinction between these two materials was the presence of steel fibres in UHPC, as neither contained coarse aggregates. Kim et al. [46] found out that deeper and more severe scratches on the surface of the fibres after testing them under cryogenic conditions, which indicated an improvement of their ability to resist being pulled out of the concrete.

$$\text{TDIF at } 20\ ^\circ C = \begin{cases} 0.013\log\dot{\varepsilon} + 1.078 & \dot{\varepsilon} \le 1\ s^{-1} \\ 0.975\log\dot{\varepsilon} + 0.790 & \dot{\varepsilon} > 1\ s^{-1} \end{cases} \tag{15}$$

$$\text{TDIF at } -70\ ^\circ C = \begin{cases} 0.027\log\dot{\varepsilon} + 1.160 & \dot{\varepsilon} \le 1\ s^{-1} \\ 1.356\log\dot{\varepsilon} + 0.395 & \dot{\varepsilon} > 1\ s^{-1} \end{cases} \tag{16}$$

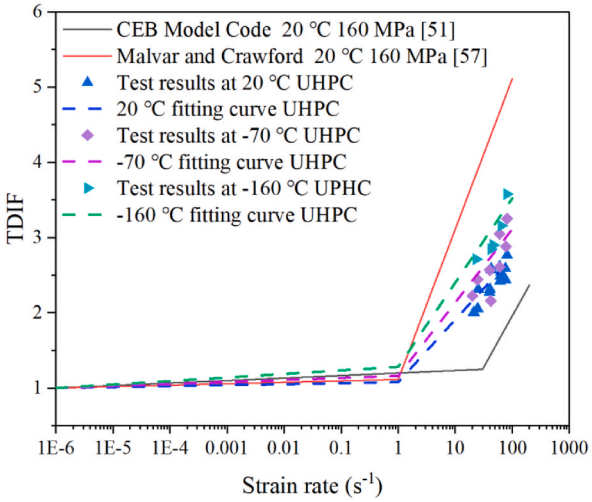

Fig. 16. TDIFs for UHPC at low temperature.

$$\text{TDIF at} -160\ ^{\circ}C = \begin{cases} 0.047\log\dot{\varepsilon} + 1.281 & \dot{\varepsilon} \le 1\ s^{-1} \\ 1.489\log\dot{\varepsilon} + 0.544 & \dot{\varepsilon} > 1\ s^{-1} \end{cases} \tag{17}$$

Like CDIFs, a single equation to predict TDIFs of UHPC was created based on experimental data in Appendix B. Fig. 17 shows the results of comparing the empirical formula with the experimental data. The coefficient of determination (R^2) for Equation (18) was 0.95, demonstrating a greater level of accuracy in predicting the TDIFs of UHPC at low temperature with various strain rate.

$$\text{TDIF} = 0.9614 - 0.002 \times T + 0.702 \times \log\dot{\varepsilon} + 0.119 \times (\log\dot{\varepsilon})^2 - 0.0005 \times T \times \log\dot{\varepsilon} \tag{18}$$

where T stands for temperature in °C, $-160\ ^{\circ}\text{C} \le T \le 20\ ^{\circ}\text{C}$; $\dot{\varepsilon}$ represents as the strain rate, $19.89\ \text{s}^{-1} \le \dot{\varepsilon} \le 81.32\ \text{s}^{-1}$.

7. Limitations

While this study provides valuable information about UHPCs' dynamic behaviour at low and cryogenic temperatures, it is important to acknowledge its limitations. The research primarily focused on macroscopic mechanical properties and did not delve deeply into the microstructural mechanisms underlying the observed dynamic behaviour. Advanced microstructural characterisation techniques such as X-ray computed tomography (CT) scanning and Scanning Electron Microscopy (SEM) would be beneficial for future studies to provide a more comprehensive understanding of the material's behaviour. CT scanning could enable three-dimensional visualisation and quantification of internal void distribution, crack propagation patterns, and pore structure evolution at different temperatures. Similarly, high-resolution SEM analysis would allow detailed examination of the interfacial transition zone (ITZ)

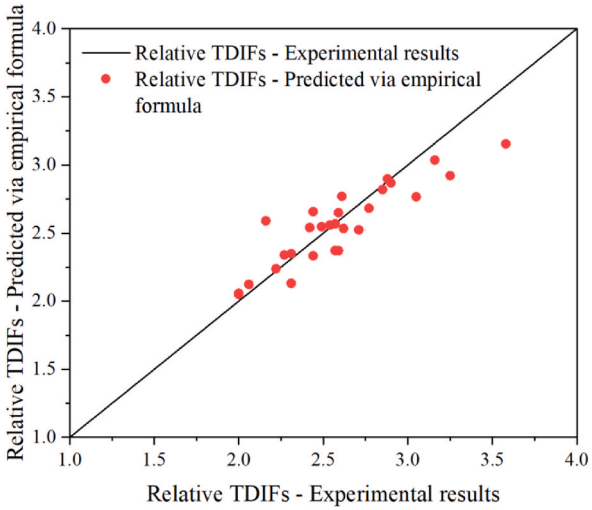

Fig. 17. Comparison of predicted TDIFs to experimental results.

between aggregates and cement paste, revealing potential microstructural changes, ice crystal formation mechanisms, and their impact on bond strength at cryogenic temperatures. Such advanced imaging techniques would help establish direct correlations between microstructural alterations and the observed macroscopic mechanical properties, particularly in understanding the role of pore size distribution, ice crystallisation patterns, and ITZ degradation in the dynamic response of UHPC under extreme temperature conditions.

8. Conclusions

In view of the comprehensive experimental investigation presented in current study, several key conclusions can be drawn regarding the dynamic behaviour of UHPC at low and cryogenic temperatures:

- UHPC exhibited superior resistance to damage and fragmentation, especially under dynamic loading conditions at low temperatures. The failure patterns of UHPC were characterised by more localised cracking and reduced disintegration, even at high strain rates and cryogenic temperatures.
- The dynamic compressive strength of UHPC increased significantly with strain rate across all temperature conditions. However, the rate of strength increase slowed down at higher strain rates (above 120 s^{-1}). At a given strain rate, the dynamic compressive strength of UHPC was higher at the lower temperatures, with the highest strength observed at −160 °C.
- The dynamic compressive elastic modulus of UHPC exhibited a complex relationship with temperature. It was the highest at −70 °C owing to the ice filling and binding effects within the concrete pores, but decreased at −160 °C resulting from the thermal expansion mismatch between the UHPC constituents.
- Under dynamic splitting tensile loading, UHPC displayed a transition in failure modes from shear failure at lower strain rates to tensile failure at higher strain rates. The damage severity was more pronounced at lower temperatures (−70 and −160 °C) in comparison with room temperature.
- The relationships between dynamic compressive and splitting tensile strength at various temperature were carried out.
- DIFs in compression of UHPC decreased with decline in temperature, indicating reduced strain rate sensitivity at lower temperatures. In contrast, DIFs in tension of UHPC increased when the temperature went down.

In conclusion, UHPC demonstrated superior performance in terms of ductility, controlled failure modes, and reduced strain rate sensitivity under dynamic loading conditions at low and extremely low temperatures. This rendered UHPC a more suitable material for concrete infrastructure subjected to coupled extreme environmental and loading conditions, such as those encountered in cryogenic storage facilities or other harsh environments.

CRediT authorship contribution statement

Kaiyi Chi: Writing – original draft, Methodology, Investigation, Formal analysis, Data curation. **Jun Li:** Writing – review & editing, Methodology, Investigation. **Ruizhe Shao:** Methodology, Data curation. **Jian Liu:** Methodology, Investigation. **Zhongxian Liu:** Methodology, Investigation. **Chengqing Wu:** Writing – review & editing, Resources, Project administration, Methodology, Investigation, Funding acquisition, Formal analysis, Data curation, Conceptualization.

Declaration of competing interest

The authors declare that they have no known competing financial interests or personal relationships that could have appeared to influence the work reported in this paper.

Acknowledgement

The study presented in this study is supported by the ARC Discovery Grant DP210101100.

Appendix A. Dynamic compression SHPB test results of UHPC at 20, -70 and −160 °C

Temperature (T)	Strain rate (s^{-1})	Dynamic compressive strength ($f'_{c,d}$)	CDIF
20 °C	38.50	191.18	1.19
	40.72	187.66	1.16
	41.01	189.86	1.18
	77.20	204.88	1.27
	71.70	202.05	1.25
	81.38	212.75	1.32
	103.15	221.32	1.37
	119.09	236.13	1.46

(*continued on next page*)

(*continued*)

Temperature (T)	Strain rate (s^{-1})	Dynamic compressive strength ($f'_{c,d}$)	CDIF
	118.90	236.52	1.47
	120.09	237.40	1.47
	158.23	245.12	1.52
	162.60	233.20	1.45
	165.81	250.86	1.56
−70 °C	39.06	203.57	1.05
	52.07	218.03	1.13
	81.57	237.81	1.23
	78.24	237.50	1.23
	75.03	243.05	1.26
	83.30	250.36	1.29
	121.25	260.66	1.35
	119.66	265.46	1.37
	114.72	260.48	1.35
	161.10	261.91	1.35
	162.55	266.51	1.38
−160 °C	45.22	215.09	1.02
	50.04	225.70	1.07
	82.32	239.35	1.13
	88.86	244.11	1.15
	119.21	268.09	1.27
	122.82	262.51	1.24
	161.49	274.53	1.30

Appendix B. Dynamic splitting tensile SHPB test results of UHPC at 20, -70 and −160 °C

Temperature (T)	Strain rate (s^{-1})	Dynamic splitting tensile strength ($f't,d$)	TDIF
20 °C	20.99	15.02	2.00
	21.39	15.01	2.00
	24.79	15.43	2.06
	25.24	17.34	2.31
	39.89	17.06	2.27
	40.63	17.36	2.31
	42.71	19.39	2.59
	42.82	19.29	2.57
	60.02	19.63	2.62
	60.84	18.14	2.42
	61.68	18.65	2.49
	63.22	19.05	2.54
	76.20	19.42	2.59
	77.38	18.28	2.44
	81.32	20.74	2.77
−70 °C	19.89	22.52	2.22
	24.51	24.71	2.44
	40.11	25.98	2.57
	41.98	21.85	2.16
	59.99	30.86	3.05
	60.40	26.42	2.61
	77.61	29.15	2.88
	81.38	32.91	3.25
−160 °C	23.29	30.51	2.71
	42.33	32.02	2.85
	46.58	32.63	2.90
	64.34	35.52	3.16
	80.48	40.22	3.58

Data availability

Data will be made available on request.

References

[1] N. Krstulovic-Opara, Liquefied natural gas storage: material behavior of concrete at cryogenic temperatures, ACI Mater. J. 104 (3) (2007) 297.
[2] R.B. Kogbara, S.R. Iyengar, Z.C. Grasley, E.A. Masad, D.G. Zollinger, A review of concrete properties at cryogenic temperatures: towards direct LNG containment, Construct. Build. Mater. 47 (2013) 760–770.
[3] L. Dahmani, A. Khenane, S. Kaci, Behavior of the reinforced concrete at cryogenic temperatures, Cryogenics 47 (9–10) (2007) 517–525.
[4] X. Liu, M.-H. Zhang, K.S. Chia, J. Yan, J.R. Liew, Mechanical properties of ultra-lightweight cement composite at low temperatures of 0 to− 60° C, Cement Concr. Compos. 73 (2016) 289–298.
[5] G. Lee, T. Shih, K.-C. Chang, Mechanical properties of concrete at low temperature, J. Cold Reg. Eng. 2 (1) (1988) 13–24.
[6] Y. Goto, T. Miura, Mechanical properties of concrete at very low temperatures, in: Proceedings of 21st Japan Congress on Materials Research, 1978.
[7] T. Miura, The properties of concrete at very low temperatures, Mater. Struct. 22 (4) (1989) 243–254.
[8] F. Rostasy, G. Wiedemann, Stress-strain-behaviour of concrete at extremely low temperature, Cement Concr. Res. 10 (4) (1980) 565–572.
[9] D.E. Berner, Behavior of Prestressed Concrete Subjected to Low Temperatures and Cyclic Loading (Cryogenic, Offshore), University of California, Berkeley, 1984.
[10] F. Rostásy, U. Pusch, Strength and deformation of lightweight concrete of variable moisture content at very low temperatures, Int. J. Cem. Compos. Lightweight Concr. 9 (1) (1987) 3–17.
[11] V. Van de Veen, Properties of Concrete at Very Low Temperatures: A Survey of the Literature, 1987. Report Stevin Laboratory, Concrete Structures 25-87-2.
[12] H. Lin, Y. Han, S. Liang, F. Gong, S. Han, C. Shi, P. Feng, Effects of low temperatures and cryogenic freeze-thaw cycles on concrete mechanical properties: a literature review, Construct. Build. Mater. 345 (2022) 128287.
[13] Y. Huo, H. Sun, D. Lu, Z. Chen, Y. Yang, Mechanical properties of concrete at low and ultra-low temperatures-a review, J. Infrastruct. Preservat. Resili. 3 (1) (2022) 20.
[14] M. Amran, S.-S. Huang, A.M. Onaizi, N. Makul, H.S. Abdelgader, T. Ozbakkaloglu, Recent trends in ultra-high performance concrete (UHPC): current status, challenges, and future prospects, Construct. Build. Mater. 352 (2022) 129029.
[15] M.-J. Kim, D.-Y. Yoo, S. Kim, M. Shin, N. Banthia, Effects of fiber geometry and cryogenic condition on mechanical properties of ultra-high-performance fiber-reinforced concrete, Cement Concr. Res. 107 (2018) 30–40.
[16] M.-J. Kim, S. Kim, S.-K. Lee, J.-H. Kim, K. Lee, D.-Y. Yoo, Mechanical properties of ultra-high-performance fiber-reinforced concrete at cryogenic temperatures, Construct. Build. Mater. 157 (2017) 498–508.
[17] Y. Liu, J. Xie, J.-B. Yan, Flexural and fracture performance of UHPC exposed to low-temperature environment, Construct. Build. Mater. 373 (2023) 130865.
[18] J. Xie, Y. Liu, M.-L. Yan, J.-B. Yan, Mode I fracture behaviors of concrete at low temperatures, Construct. Build. Mater. 323 (2022) 126612.
[19] H. Zhang, B. He, X. Zhu, Q. Wang, Z. Jiang, The use of AE technique for identifying ductility degradation against cryogenic on flexural performance of UHPC at various temperature conditions, Cement Concr. Compos. 137 (2023) 104904.
[20] D.-Y. Yoo, S.-T. Kang, J.-H. Lee, Y.-S. Yoon, Effect of shrinkage reducing admixture on tensile and flexural behaviors of UHPFRC considering fiber distribution characteristics, Cement Concr. Res. 54 (2013) 180–190.
[21] L. Jin, C. Xie, W. Yu, X. Du, Effect of steel fiber content on failure strength and toughness of UHPC-CA at low temperature: an experimental investigation, J. Build. Eng. (2024) 109976.
[22] Q. Yu, W. Zhuang, C. Shi, Research progress on the dynamic compressive properties of ultra-high performance concrete under high strain rates, Cement Concr. Compos. 124 (2021) 104258.
[23] D. Zhang, H. Tu, Y. Li, Y. Weng, Effect of fiber content and fiber length on the dynamic compressive properties of strain-hardening ultra-high performance concrete, Construct. Build. Mater. 328 (2022) 127024.
[24] G. Ren, H. Wu, Q. Fang, J. Liu, Effects of steel fiber content and type on dynamic compressive mechanical properties of UHPCC, Construct. Build. Mater. 164 (2018) 29–43.
[25] Z. Rong, W. Sun, Y. Zhang, Dynamic compression behavior of ultra-high performance cement based composites, Int. J. Impact Eng. 37 (5) (2010) 515–520.
[26] R.J. Thomas, A.D. Sorensen, Review of strain rate effects for UHPC in tension, Construct. Build. Mater. 153 (2017) 846–856.
[27] S. Gurusideswar, A. Shukla, K.N. Jonnalagadda, P. Nanthagopalan, Tensile strength and failure of ultra-high performance concrete (UHPC) composition over a wide range of strain rates, Construct. Build. Mater. 258 (2020) 119642.
[28] Y. Yao, F.A. Silva, M. Butler, V. Mechtcherine, B. Mobasher, Tensile and flexural behavior of ultra-high performance concrete (UHPC) under impact loading, Int. J. Impact Eng. 153 (2021) 103866.
[29] Y. Su, J. Li, C. Wu, P. Wu, Z.-X. Li, Effects of steel fibres on dynamic strength of UHPC, Construct. Build. Mater. 114 (2016) 708–718.
[30] Z. Wu, C. Shi, W. He, D. Wang, Static and dynamic compressive properties of ultra-high performance concrete (UHPC) with hybrid steel fiber reinforcements, Cement Concr. Compos. 79 (2017) 148–157.
[31] X. Hou, S. Cao, W. Zheng, Q. Rong, G. Li, Experimental study on dynamic compressive properties of fiber-reinforced reactive powder concrete at high strain rates, Eng. Struct. 169 (2018) 119–130.
[32] S. Cao, X. Hou, Z. Dong, Experimental study on dynamic direct tensile performances of steel fiber-reinforced RPC at high strain rates, J. Build. Eng. (2024) 109673.
[33] J. Liu, X. Dai, X. Yu, C. Yao, X. Zhao, D. Kong, Tensile behaviour and full-field strain of reactive powder concrete under dynamic loading: effects of fibre length and content, Construct. Build. Mater. 416 (2024) 135008.
[34] T.J. MacLean, A. Lloyd, High strain rate and low temperature effects on the compressive behaviour of concrete, Int. J. Prot. Struct. 12 (1) (2021) 73–94.
[35] Y. Qiao, H. Wang, L. Cai, W. Zhang, B. Yang, Influence of low temperature on dynamic behavior of concrete, Construct. Build. Mater. 115 (2016) 214–220.
[36] L. Jin, K. Liu, R. Zhang, W. Yu, X. Du, X. Deng, Combined effects of cryogenic temperature and strain rates on compressive behavior of concrete, Int. J. Damage Mech. 31 (9) (2022) 1396–1419.
[37] H. Su, Z. Zhu, T. Li, H. Xiang, Experimental studies and numerical analysis of the dynamic mechanical properties of concrete at low temperatures, Construct. Build. Mater. 404 (2023) 133221.
[38] K. Chi, J. Li, R. Shao, L. Chen, S. Xu, C. Wu, Experimental study on impact behaviour of normal strength mortar at cryogenic temperatures and after freeze-thaw cycles, Construct. Build. Mater. 440 (0950–0618) (2024) 137497.
[39] P. Follansbee, C. Frantz, Wave propagation in the split Hopkinson pressure bar, J. Eng. Mater. Technol. (1983) 105.
[40] H. Kolsky, An investigation of the mechanical properties of materials at very high rates of loading, Proc. Phys. Soc. B 62 (11) (1949) 676.
[41] U. Lindholm, Some experiments with the split hopkinson pressure bar*, J. Mech. Phys. Solid. 12 (5) (1964) 317–335.
[42] C. Shi, Z. Wu, J. Xiao, D. Wang, Z. Huang, Z. Fang, A review on ultra high performance concrete: Part I. Raw materials and mixture design, Construct. Build. Mater. 101 (2015) 741–751.
[43] Z. Wu, C. Shi, K.H. Khayat, L. Xie, Effect of SCM and nano-particles on static and dynamic mechanical properties of UHPC, Construct. Build. Mater. 182 (2018) 118–125.
[44] S.M. Mousavi, M.M. Ranjbar, R. Madandoust, Combined effects of steel fibers and water to cementitious materials ratio on the fracture behavior and brittleness of high strength concrete, Eng. Fract. Mech. 216 (2019) 106517.
[45] B. He, H. Zhang, X. Zhu, Q. Zheng, O. Onuaguluchi, N. Banthia, Z. Jiang, Thermal-dependent brittleness effect of ultra-high performance concrete exposed to cryogenic flexural loads by acoustic emission evaluation, Cement Concr. Compos. 139 (2023) 105056.
[46] M.-J. Kim, D.-Y. Yoo, Cryogenic pullout behavior of steel fibers from ultra-high-performance concrete under impact loading, Construct. Build. Mater. 239 (2020) 117852.
[47] X. Wu, V. Prakash, Dynamic compressive behavior of ice at cryogenic temperatures, Cold Reg. Sci. Technol. 118 (2015) 1–13.

[48] D. Zhang, J. Niu, P. Chen, P. Ranjith, W. Nie, Mechanical properties of concrete under different water content and low temperature conditions, Mater. Struct. 56 (4) (2023) 71.
[49] M. Khan, M. Iqbal, Strain rate and size effects on dynamic tensile behaviour of standard and high-strength concrete: an experimental study, in: Structures, Elsevier, 2024.
[50] D. Hobbs, The tensile strength of rocks, in: International Journal of Rock Mechanics and Mining Sciences & Geomechanics Abstracts, Elsevier, 1964.
[51] CEB-FIP, Model Code 1990 for Concrete Structures, Comit e Euro-International du B eton and F ed eration Internationale de la Pr econtrainte, Thomas Telford, London, 1993.
[52] Y. Guo, G. Gao, L. Jing, V. Shim, Response of high-strength concrete to dynamic compressive loading, Int. J. Impact Eng. 108 (2017) 114–135.
[53] T. Ngo, P. Mendis, A. Whittaker, A rate dependent stress-strain relationship model for normal, high and ultra-high strength concrete, Int. J. Prot. Struct. 4 (3) (2013) 451–466.
[54] J. Zhengwu, D. Zilong, Z. Xinping, L. Wenting, Increased strength and related mechanisms for mortars at cryogenic temperatures, Cryogenics 94 (2018) 5–13.
[55] G. Wiedemann, *Zum Einfuss Tiefer Temperaturen auf Festigkeitund Verformung von Beton* in *Institute for Building Materials, Solid Construction, and Fire Protection*, Technical University of Braunschweig, 1982.
[56] D. Huang, Y. Feng, Q. Xia, J. Tian, X. Li, Research on mechanical properties and durability of early frozen concrete: a review, Construct. Build. Mater. 425 (2024) 135988.
[57] L.J. Malvar, J.E. Crawford, Dynamic increase factors for concrete, DTIC document 1 (1.4) (1998) 1.6.
[58] S.H. Park, D.J. Kim, S.W. Kim, Investigating the impact resistance of ultra-high-performance fiber-reinforced concrete using an improved strain energy impact test machine, Construct. Build. Mater. 125 (2016) 145–159.
[59] L. Yang, X. Lin, R.J. Gravina, Evaluation of dynamic increase factor models for steel fibre reinforced concrete, Construct. Build. Mater. 190 (2018) 632–644.